Bubble mapping: three-dimensional visualisation of gas–liquid flow regimes using electrical tomography

OPEN ACCESS
IOP Publishing
Measurement Science and Technology
Meas. Sci. Technol. **30** (2019) 045303 (13pp)
https://doi.org/10.1088/1361-6501/ab06a9

Bubble mapping: three-dimensional visualisation of gas–liquid flow regimes using electrical tomography

Qiang Wang[1,2], **Xiaodong Jia**[1] **and Mi Wang**[1]

[1] School of Chemical and Process Engineering, University of Leeds, Leeds LS2 9JT, United Kingdom
[2] School of Chemistry, University of Edinburgh, Edinburgh EH9 3FJ, United Kingdom

E-mail: m.wang@leeds.ac.uk

Received 30 October 2018, revised 8 February 2019
Accepted for publication 12 February 2019
Published 14 March 2019

Abstract

It is well known that electrical tomography is capable of 'seeing' through opaque pipe walls and flow media. However, due to the relatively low spatial resolution, electrical tomograms are ineffective on visualisation of small bubbles or sharp interfaces between large bubbles and the liquid. These limitations give rise to ambiguity in human and/or machine perception of flow dynamics from presenting bubble cluster and blurry boundaries of large bubbles in faint colour or grey. In this paper, a binary approach, called bubble mapping, is proposed to enhance the visibility of flow regime in gas–liquid pipeline flows. With the input gas concentration tomograms reconstructed by an electrical tomography, the method takes the major visual characteristics of typical flow regimes in common recognition as a prior knowledge and replaces the conventional colour mapping with a number of bubbles and their mergence with a thresholding value. With this approach, a stack of cross-sectional tomograms by electrical tomography is transformed and displayed as a collection of individual gas bubbles. The transformation is done with the help of a lookup table indexed by bubble size and an enhanced isosurface algorithm for vivid three-dimensional visualisation. This new approach has been applied to a gas-in-water flow rig and its performance is compared with photo images taken by a high-speed camera. Reasonable agreements have been obtained for common flow regimes including bubbly flow, stratified flow, plug flow, slug flow and annular flow in horizontal pipe and bubbly flow, slug flow and annular flow in vertical pipe. Results evidence the method can provide a photorealistic flow visualisation and therefore enhance the visibility of electrical tomograms for visual identification of flow regime, particularly for opaque media in industrial flows.

Keywords: electrical tomography, flow regimes, gas–liquid flow, bubble size, bubble boundary, bubble mapping, 3D visualisation

(Some figures may appear in colour only in the online journal)

1. Introduction

Gas–liquid two-phase flow is a common phenomenon in industries, such as nuclear, pharmaceutical and gas-oil industries. The primary purpose of visualising flow in pipeline, in more general terms, is to understand flow dynamics for enhancing the process safety, production rate and quality. Spatial and/or temporal distributions of gas and liquid phases in pipeline, i.e. flow regimes are crucial for design, analysis, and operation of two-phase flow systems [2]. Due to the complexity of the interaction between gas and liquid, as well as the impacts of physical and fluid properties, such as channel inclination, surface tension, an infinite number of flow structures could occur in a given channel. Fortunately, when a gas–liquid flow

is in a steady state, i.e. the flow with certain flowrate of each phase is fully developed, flow regimes can be simply categorised into a few different forms depending on pipe orientation. Flow regime map can be derived to describe possible flow regimes with certain pipe orientation. Figure 1 demonstrates flow regime maps and typical flow regimes for vertical and horizontal gas–liquid pipeline flow.

The dynamics of multiphase flow are of vital importance since they significantly influence the optimal design parameters and the operational conditions of the industries containing multiphase flow [3]. Sudden changes of flow patterns in production pipe could have adverse effect on productivity, the pipe itself, and the instruments associated with the production system. Therefore, flow regime visualisation has attracted many attentions from scientists and engineers. The method of observation with a high-speed camera may be the most common one to reveal the spatial distribution of gas in water. This observation, however, is subject to the availability of the optical transparency of pipe wall and the continuous phase in fluids. Moreover, the void fraction of gas phase also affects the quality of the observation (e.g. $\geqslant$10% [4]). Other alternative non-intrusive method, e.g. gamma-ray tomography, is rarely applied due to its limits as its cost, installation and safety. Therefore, an effective and feasible method is highly demanded.

Process tomography has been widely applied to measure and visualise multiphase flow in the past few decades. Particularly, electrical tomography is a type of visualisation techniques based on the phase difference in electrical properties, e.g. conductivity or permittivity [3]. Compared with other tomographic techniques, electrical tomography, e.g. electrical resistance tomography (ERT) or electrical capacitance tomography (ECT), is capable of producing cross-sectional images with a relatively high temporal resolution (sub-millisecond) [5–7] but a relatively low spatial resolution (e.g. around 5%, i.e. the ratio of the smallest size of identifiable objects to the diameter of the sensor) [8]. Electrical resistance tomography, as a typical electrical tomography, includes a sensor consist of a number of electrodes for injecting current into and measuring voltage drops from the boundary of process medium under the investigation, a signal conditioner and data acquisition system and an algorithm to reconstruct the conductivity distribution in the medium [9]. Generally, the local conductivity in tomogram has to be translated to an engineering data, e.g. signing gas concentration to an imaging pixel in the study, which can be converted with Maxwell relationship [10]. Algorithms can be generally categorised to one-step or multistep iterative algorithms based on the computation speed, or qualitative or quantitative algorithms based on the reconstructed data accuracy [9]. The third type of algorithms may include those based on a prior knowledge [11], statistical [12, 13] or artificial intelligent [14] approaches, which presents their specific features and limits. In this study, we are focusing on the enhancement of flow visualisation from reconstructed tomograms which were reconstructed with the modified sensitivity back-projection algorithm (MSBP), a one-step algorithm [15]. It is expected the principle of method discussed in this paper can be applied to tomograms reconstructed with other algorithm.

Among the visualisation techniques for scalar fields, the method of colour mapping is the most widely applied, owing to its simplicity in computation and implementation [16]. The basic idea behind the colour mapping is to convert different scalar values to different colours according to a predefined lookup table. From visualisation and perception viewpoints, applying a lookup table should emphasise important characteristics, but reduce less important or irrelevant information to the minimum. However, the colour mapping-based images in electrical tomography are unable to reveal sufficient flow characteristics, e.g. a low concentration of small bubbles in a common colour (figure 2(a)), owing to the incapability of electrical tomography to report the conductivity change over a region as stated previously. The faint change in colour mapping due to the small bubbles present a challenge for human visibility. In addition, the images are strongly affected by the definition of the lookup table, which may result in ambiguity for human and machine perception (figure 2(b)), e.g. bubble boundary.

In addition to the aforementioned approaches, there are a few different approaches for the visualisation. In [4], wire-mesh sensor (WMS) was used for measuring bubble size and distribution in air-water flow in a vertical vessel, without the involvement of reconstruction process, i.e. on raw data. In Prasser's method, a bubble is reconstructed by firstly locating the centre of a bubble, and then swarming the neighbouring pixels around the centre to form the bubble. However, the result may tend to be an overestimation of bubble size. When applying to electrical tomograms, this method is unable to identify small bubbles due to the relatively low spatial resolution of the tomograms. Another example is the application of raytracing technique by [17], which works by tracing a path from an imaginary eye through each pixel in a virtual screen, and calculating the colour of the object visible through it [16]. Since bubbles in electrical tomograms are not clearly presented, the ray is unable to interact with individual objects, i.e. bubbles, and hence raytracing is not directly applicable to electrical tomograms. [18] applied conventional texture-based volume rendering technique in computer graphics to achieve real-time 3D visualisation on ECT tomograms, which essentially displays 3D volume data in a 2D image by projection. Again, this method does not manage to reflect adequate flow dynamics involving small bubbles.

In this paper, a new approach is proposed to enhance the capability of electrical tomography to visualise gas–liquid pipeline flows. It is assumed that as fully-developed flow, bubble sizes proportional to local mean volume fractions, small bubbles are spherical while large bubbles are random in shape, and the growth and collapse of bubbles are ignored [1, 2]. With the assumptions, a bubble lookup table is defined to replace the conventional colour lookup table. By remeshing the original dataset with temporal and spatial information into a structured space consisting of uniform cubes, the bubble lookup table can be applied to reconstruct small bubbles with a visible size but keeping the concentration the same as the

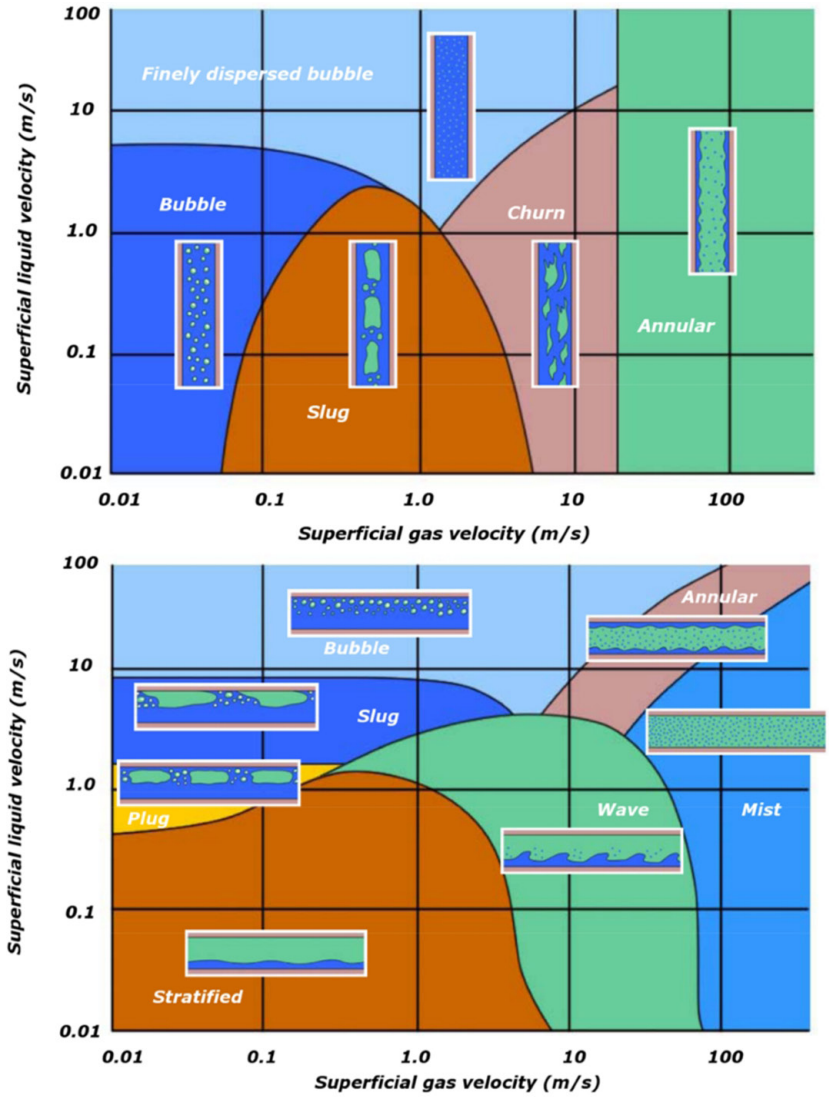

Figure 1. Flow regime maps and typical flow regimes in vertical (the top) and horizontal (the bottom) pipes. Reproduced with permission from [1].

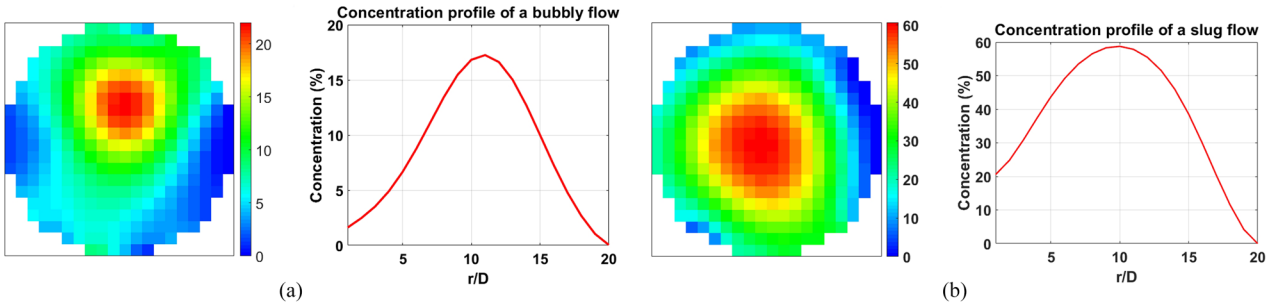

Figure 2. ERT-based gas concentration tomograms and profiles of a bubbly flow (a) and a slug flow (b) reconstructed with MSBP.

original value in the cube. Large bubbles can also be located by merging a swarm of adjacent cubes with mean volume fractions beyond a carefully-selected threshold. Later, an enhanced isosurface method is utilised to identify the boundaries between large bubbles and the liquid phase.

The rest of the paper is arranged as follows. The methodology is introduced in section 2, and the visualisation results are presented in section 3. Then, conclusions are made in section 4, along with brief discussions of the benefits and limitations of the approach.

2. Methodology

In our study, a 16-electrode ERT is deployed. The number of independent measurements is 114, whereas the number of the unknown pixel resistance is 316. The image reconstruction

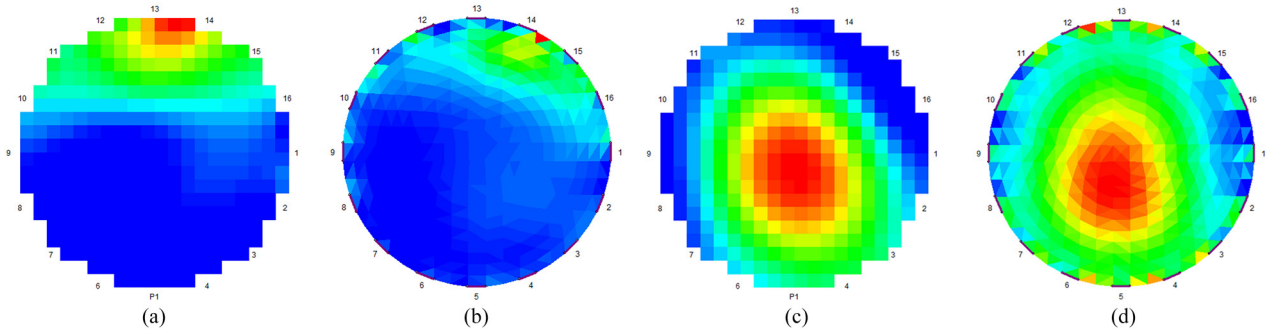

Figure 3. ERT-based concentration tomograms of bubbly flow by (a) MSBP and (b) SCG, and slug flow by (c) MSBP and (d) SCG.

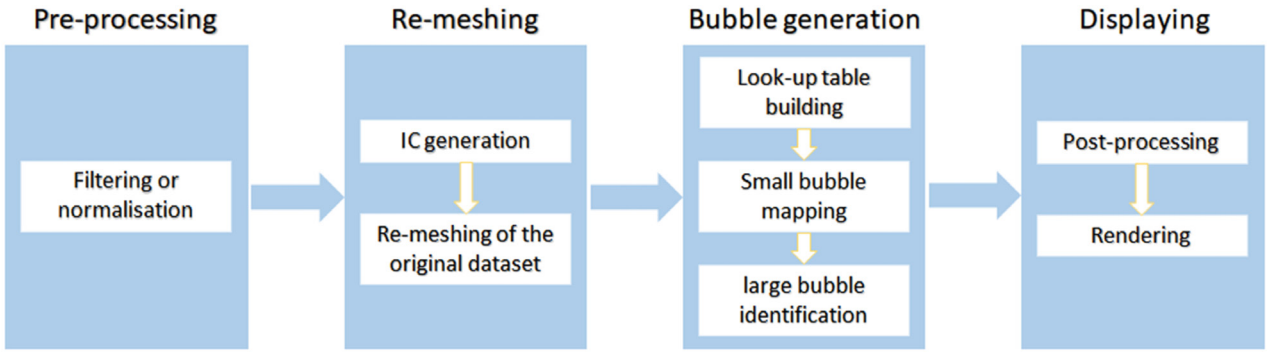

Figure 4. The pipeline of the new approach.

therefore is to derive the 316 unknowns from the 114 measurements. The non-linearity makes the precise derivation of the unknowns extremely challenging, even advanced iterative reconstruction algorithm is applied. Figure 3 presents the ERT concentration tomograms of small bubbles (figures 3(a) and (b)) and large bubbles (figures 3(c) and (d)) reconstructed by MSBP and sensitivity-based conjugate gradient (SCG) method [15]. The images clearly demonstrate the limitations of electrical tomography when visualising multiphase flow. That is, they are unable to identify small bubbles below a certain size or to indicate the sharp interface between the dispersed phase (e.g. gas) and the continuous phase (e.g. water). Nevertheless, despite its low spatial resolution, it has been reported, in terms of ERT, that it is capable of handling gas concentration close to 100% for a gas-water flow [19].

Conventionally, the colour of each pixel in electrical tomograms is determined by the corresponding concentration value of the pixel. For the convenience in discussion, the concentration value at the imaging pixel is dimensionlessly defined as 0% or 100%, corresponding to a pixel fully occupied by liquid or gas. Otherwise, the pixel concentration is within the range (0%, 100%), meaning the pixel is partially filled by gas. Following the same concept, a new lookup table can be established, in which a concentration value is transferred to a spherical bubble within a cell, but the concentration value is maintained by the ratio of the areas of the spherical bubble against the cell. In order to reconstruct bubbles correctly, both spatial and temporal dimensional information have to be taken into account, by means of properly defining the dimension of interrogation cell (IC). Based on the dimensional definition of IC, the original concentration space is split into a coarser regular grid, to which a new lookup table is applied to reconstruct small bubbles, while indicating the rough locations of large bubbles. Afterwards, an enhanced isosurface algorithm is utilised to identify the boundary between large bubbles and liquid. Finally, when both small bubbles and large bubbles are generated, they are displayed by the common approach in computer graphics. Figure 4 shows the steps of the new approach, and each step will be addressed in the following sections.

2.1. Data pre-processing

Due to unavoidable noise during measurement, the converted concentration distribution from conductivity distribution may contain abnormal data, e.g. negative values. Therefore, it has to be filtered firstly. The filtered distribution is then split into IC by incorporating both spatial and temporal dimensional information into the definition of the cells. In particular, spatial information needs to consider the size of small bubbles in real situation, as well as the resolution capability of the systems, while temporal information needs to incorporate actual velocity of gas phase and data acquisition speed of the employed systems into IC definition.

Given a set of real numbers R, a concentration set is defined as:

$$C = \{c_i\} \quad c_i \in R. \tag{1}$$

The set C may need to be filtered/normalised to fit into meaningful range, i.e. (0%, 100%). When the software [20] that was employed for the reconstruction process to generate stacked concentration tomograms provides a non-shifted mean concentration, the pixel concentrations are always within the range (0%, 100%) with some internal restrictions

of the algorithm in the software, in which case filtering/normalisation is not required. Otherwise, a simple filter is defined by (2):

$$F(c_i) = \begin{cases} 0. & c_i < 0 \\ c_i & 0 \leqslant c_i \leqslant 100 \\ 100 & c_i > 100. \end{cases} \tag{2}$$

When the filtering in the approach is required, a shift of averaged concentration with and without it may be introduced. However, the difference is actually too little to affect the quality of visualisation, and therefore the error is treated as ignorable.

2.2. Data re-meshing

In ERT, there are two important criteria, namely spatial and temporal resolution, for evaluating the quality of ERT tomograms. They refer to the precision of ERT measurement with respect to space and time. The spatial resolution of ERT is down to 5% of vessel size [8], whereas the temporal resolution varies depending on the hardware. Accordingly, for a pipe with diameter D_p, the minimum size D_m is $D_\mathrm{m} = 0.05 \times D_\mathrm{p}$. On the other hand, when a gas–liquid flow is fully developed, the largest size of small bubbles can be observed and estimated. For example, when pipe diameter is within 50 mm −200 mm, the largest size is approximately less than 20 mm [21–24]. It is worth noting that the primary purpose of remeshing is to generate small bubbles missing in ERT tomograms. Together the spatial resolution of ERT and the assumption of the small bubble size, the spatial dimension of IC can therefore be defined as:

$$\mathrm{Dim}_\mathrm{s}^\mathrm{IC} = \mathrm{Dim}_{\mathrm{s},x}^\mathrm{IC} \times \mathrm{Dim}_{\mathrm{s},y}^\mathrm{IC} = \frac{\max\{D_\mathrm{s}, D_\mathrm{m}\}}{\frac{D_\mathrm{p}}{m}} \times \frac{\max\{D_\mathrm{s}, D_\mathrm{m}\}}{\frac{D_\mathrm{p}}{n}} \tag{3}$$

where $\mathrm{Dim}_{\mathrm{s},x}^\mathrm{IC}$ and $\mathrm{Dim}_{\mathrm{s},y}^\mathrm{IC}$ are the spatial dimension $\mathrm{Dim}_\mathrm{s}^\mathrm{IC}$ of IC at x and y axis respectively, D_s is the maximal diameter of small bubbles, and D_p is the diameter of the pipe containing the flow, m and n is the spatial grid definition of the original concentration set.

It is particularly noted that the third dimension of the input tomographic dataset generally only reflects temporal information (imaging speed), rather than spatial information. It therefore needs to be transferred to spatial information by incorporating local velocity of gas phase with sufficient data acquisition speed of the tomography. For instance, suppose the local velocity of the gas phase is 1 m s^{-1}, and hardware collection speed is 1000 fps, the collected 1000 frames need to reflect the one-meter movement of the gas phase if the measurement is taken for one second. That is, within the time for collecting two consecutive frames, i.e. 1/1000 = 1 ms, the flow actually moves forward 1 m s^{-1} × 1 ms = 1 mm. Therefore, the temporal dimension of IC can be defined as:

$$\mathrm{Dim}_t^\mathrm{IC} = \frac{\max\{D_\mathrm{s}, D_\mathrm{m}\}}{v \times \Delta t} \tag{4}$$

where v is the local velocity of the gas phase, and Δt is the temporal resolution of the original concentration set.

Ideally, the velocity should contain the one for every bubble since each bubble may have different velocity. For example, concentration, velocity field, and other information are usually utilised together to for the derivation and evolution of bubble size and distribution in multiphase flow simulation [25]. Unfortunately, velocity field is hardly available in tomography-based flow characterisation. Instead, statistics-based methods, e.g. cross correlation [26] are applied to derive the axial velocity as an approximation of the individual velocity of each bubble, with the assumption that the velocities at other directions are ignored. Given an ERT system with two parallel-installed electrode arrays along pipeline, gas velocity can be derived with a direct cross correlation method using the following equation:

$$R_{1,2}(n) = \sum_{m=n+1}^{N} f_1(m-n) \times f_2(m) \qquad n = 0, 1, ..., (N-1) \tag{5}$$

where 1 and 2 in $R_{1,2}(n)$ are the down-stream and up-stream sensor planes, N is the sample length, and $f_i(m)$ is the mth tomograms from ith planes of sensors. (5) is the general form of cross-correlation method for process tomography to seek for the correlation [27, 28]. (5) is further adapted in [29] to become suitable for online calculation by updating $R_{12}(n)$ with the new kth tomograms, given by (6):

$$R_{1,2}^{(k)}(n) = R_{12}^{(k-1)} + f_1(k-n) \times f_2(k) \qquad n = 0, 1, ..., (N-1) \tag{6}$$

where superscript (k) indicates that the related value is the kth sample. The major difference between (5) and (6) is that the former uses the whole input tomograms to produce mean pixel velocity distribution, whereas the latter does not, resulting in the latter presents better results. Therefore, the local velocity in this study is approximated by (6).

It is worth noting that due to the principle behind the cross-correlation method and the nature of some flow regimes, i.e. stratified (wavy) flow and annular flow in horizontal pipeline or annular flow in vertical pipeline, it is extremely challenging to extract local velocity of the gas phase with the cross-correlation method. Therefore, the velocity for these flow regimes is estimated by the superficial velocity of gas phase in this paper.

Figure 5 demonstrates an example of the calculation of IC resolution. Suppose an ERT system produces a set of electrical concentration tomograms with 20 × 20 mesh at the speed 1000 fps, pipe diameter is 100 mm, the minimum size of a bubble identified by the ERT is $D_\mathrm{m} = 0.05 \times D_\mathrm{p} = 10$ mm, and the velocity of the gas phase is 1 m s^{-1}, the $\mathrm{Dim}_\mathrm{s}^\mathrm{IC}$ can be calcualted per (3):

$$\mathrm{Dim}_\mathrm{s}^\mathrm{IC} = \frac{\max\{20, 10\}}{\frac{100}{20}} \times \frac{\max\{20, 10\}}{\frac{100}{20}} = 4 \times 4.$$

This means the original 20 × 20 tomograms need to be remeshed to $\frac{20}{4} \times \frac{20}{4} = 5 \times 5$ tomograms. Consequently, a remeshed pixel physically represents $\frac{100}{5}$ mm × $\frac{100}{5}$ mm = 20 mm × 20 mm square, i.e. the maximal diameter of the small bubbles. Accordingly, the pixel concentration of the

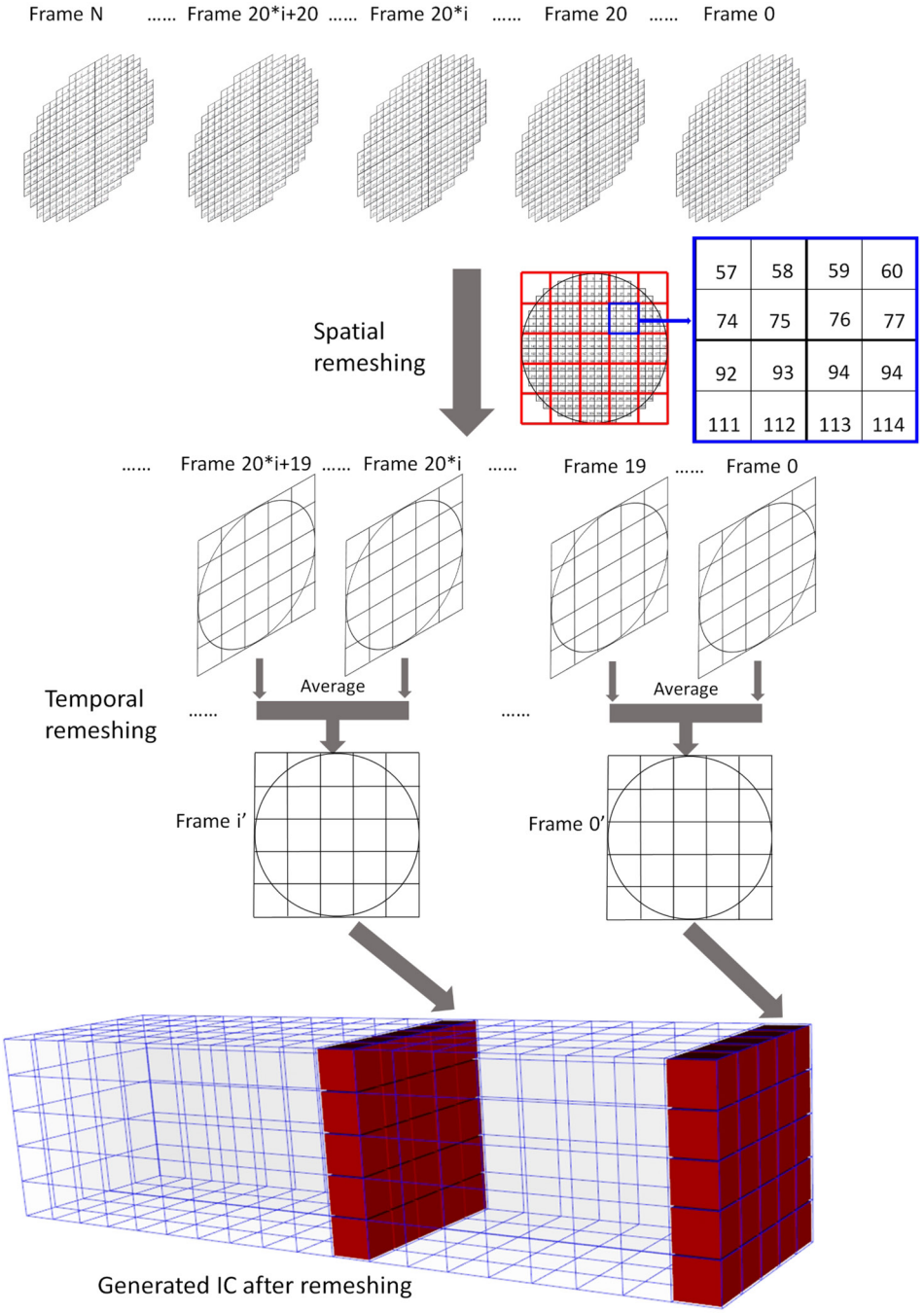

Figure 5. Example of IC resolution calculation.

spatially remeshed tomograms is calculated by averaging the pixel concentrations within the remeshed pixels, e.g. the one in the blue square (the upper part of figure 5) is by averaging the concentrations at pixel 57, 58, 59, 60, 74, 75, 76, 77, 92, 93, 94, 95, 111, 112, 113, and 114 in the original mesh and the temporal resolution of IC can be calculated per (4):

$$\mathrm{Dim}_t^{\mathrm{IC}} = \frac{\max\{0.02, 0.014\}}{1 \times \frac{1}{1000}} = 20.$$

This means that at temporal dimension, for the given conditions, during the time for the flow moving forward 20 mm, i.e. the maximal diameter of the small bubbles, 20 frames are collected by the ERT system. Therefore, every 20 tomograms need to be averaged as one frame in the temporally remeshed grid (the lower part of figure 5). It is worth pointing out that if the temporal dimension is less than 1, the actual distance the flow travels is larger than 20 mm for every two consecutive frames, and therefore interpolation is required to locate appropriate position for the flow floating 20 mm.

After the calculation of IC dimension and remeshing process, the original input tomograms are transformed to ICs (the bottom part of figure 5), and each IC physically reflects a 20 mm × 20 mm × 20 mm cube, within which a spherical

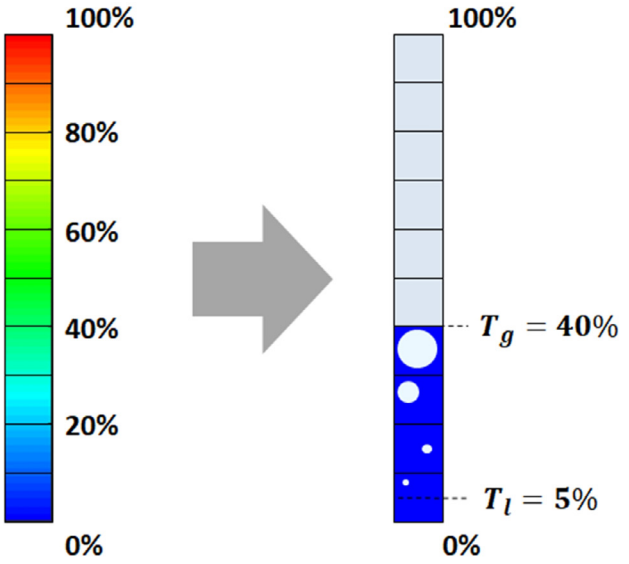

Figure 6. The new lookup table for bubble mapping in 2D.

bubble with maximal diameter 20 mm can be located in the next step.

2.3. Bubble generation

After the re-meshing, every IC is going to be processed to identify bubbles using a new lookup table (for small bubbles) and an enhance isosurface extraction algorithm (for large bubbles).

2.3.1. The new lookup table. Unlike the conventional colour-based lookup table which maps scalar value to colours, the new lookup table is to transfer scalar values to small spherical bubbles. It is usually believed that measurement error is up to 5% owing to noise [8]. In other words, when the concentration is below 5%, it is assumed only conductive phase in the pipeline, which in our case is the liquid phase. In other words, the smallest size of a bubble is based on 5% concentration of the bubble in an interrogation cell. According to [30], the threshold value of the air concentration for the transition from bubbly flow to turbulent flow in a static bubble column with a diameter of 5cm was around 40% [31]. Thereafter, as an approximated value in the paper, it is assumed when volume fraction of gas is above 40%, large bubbles appear. Consequently, 40% is used as the threshold value beyond which an IC is assumed to be full of gas. When the concentration is between 5% and 40%, there would be a small bubble inside IC, of which the size is determined by the concentration. It is worthwhile to note that this study does not intend to improve the spatial resolution of electrical tomography. Instead, it tries to represent the concentration distribution of the gas phase from the reconstructed electrical concentration tomograms in bubble terms according to the above discussion.

For gas–liquid flow, concentration of an IC is calculated as:

$$c_i^{\mathrm{IC}} = \frac{\sum_{i=1}^{m} v_i^{\mathrm{b}}}{v_i^{\mathrm{IC}}} \times 100 \tag{7}$$

where c_i^{IC} is the gas mean concentration of the cell, v_j^{b} is the volume of ith bubble inside the given volume v_i^{IC}, and m is the number of bubbles inside the volume v_i^{IC}. In the context of gas–liquid flow, it is acceptable to approximate that when an IC is reasonably small, there is only one bubble inside an IC, i.e. m is 1, thereby (7) is rewritten to:

$$c_i^{\mathrm{IC}} = \frac{v_i^{\mathrm{b}}}{v_i^{\mathrm{IC}}} \times 100 \tag{8}$$

where v_i^{b} is the volume of the bubble in ith cell. (8) can be further rearranged to:

$$v_i^{\mathrm{b}} = \frac{v_i^{\mathrm{IC}} \times c_i^{\mathrm{IC}}}{100}. \tag{9}$$

According to the dimension definition of IC, c_i^{IC} can be calculated by:

$$c_i^{\mathrm{IC}} = \frac{1}{\mathrm{Dim}_{\mathrm{s},x}^{\mathrm{IC}} \times \mathrm{Dim}_{\mathrm{s},y}^{\mathrm{IC}} \times \mathrm{Dim}_{t}^{\mathrm{IC}}} \sum_{k=1}^{\mathrm{Dim}_{t}^{\mathrm{IC}}} \sum_{j=1}^{\mathrm{Dim}_{\mathrm{s},y}^{\mathrm{IC}}} \sum_{i=1}^{\mathrm{Dim}_{\mathrm{s},x}^{\mathrm{IC}}} c_{i,j}^{k}. \tag{10}$$

By considering (3), (4), (9), and (10) altogether, the radius of the bubble with the volume v_i^{b} can be derived:

$$\begin{aligned} R_{\mathrm{b}} &= \left(\frac{3}{4\pi} \times c_i^{\mathrm{IC}} \times v_i^{\mathrm{IC}}\right)^{\frac{1}{3}} \\ &= \left(\frac{3(D_{\mathrm{s}})^3 \times \left(\sum_{k=1}^{\mathrm{Dim}_{t}^{\mathrm{IC}}} \sum_{j=1}^{\mathrm{Dim}_{\mathrm{s},y}^{\mathrm{IC}}} \sum_{i=1}^{\mathrm{Dim}_{\mathrm{s},x}^{\mathrm{IC}}} c_{i,j}^{k}\right)}{4\pi \times \mathrm{Dim}_{\mathrm{s},x}^{\mathrm{IC}} \times \mathrm{Dim}_{\mathrm{s},y}^{\mathrm{IC}} \times \mathrm{Dim}_{t}^{\mathrm{IC}}}\right)^{\frac{1}{3}}. \end{aligned} \tag{11}$$

Incorporating the assumptions into (10) as the transfer function to locate the entry of the new lookup table, and (11) as the calculation of bubble radius within an IC, the new lookup table can be established, as depicted in figure 6, in which T_g and T_l are the critical threshold values.

Further to the example in section 2.2, i.e. an IC physically reflects a 20 mm × 20 mm × 20 mm cube, the smallest size of a bubble in the cell can be derived accordingly to (11):

$$R_{\mathrm{b}} = \left(\frac{3}{4\pi} \times c_i^{\mathrm{IC}} \times v_i^{\mathrm{IC}}\right)^{\frac{1}{3}} = \left(\frac{3}{4\pi} \times 5\% \times 20\ \mathrm{mm}^3\right)^{\frac{1}{3}} = 9.8\ \mathrm{mm}$$

2.3.2. Small bubble mapping. Once the bubble-based lookup table is built, it is ready to work on the interrogated concentration data. Figure 7 demonstrates an example of the application of conventional colour mapping and new bubble mapping to 2D stacked concentration distribution. In comparison to colour-based illustration, bubble-based one is able to reveal the size and position of small bubbles. As far as the large bubble in figure 7 is concerned, the outline is already drawn, but inconsistent with the real-world situation in terms of bubble shape. This is because no consideration of merging neighbour bubbles beyond particular size has been taken. In addition, figure 7 also illustrates the existence of some unreal bubbles in the red ellipse. In consequence, the next step is to merge neighbour bubbles to form larger bubbles.

2.3.3. Large bubble identification. After the mapping, some cells may be filled with small bubbles, instead of the boundary

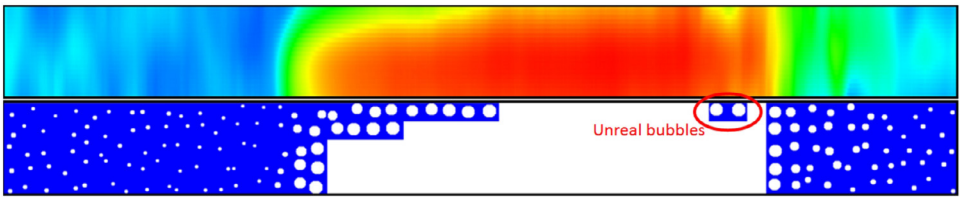

Figure 7. 2D stacked concentration tomograms by colour mapping (the top) and bubble mapping (the bottom).

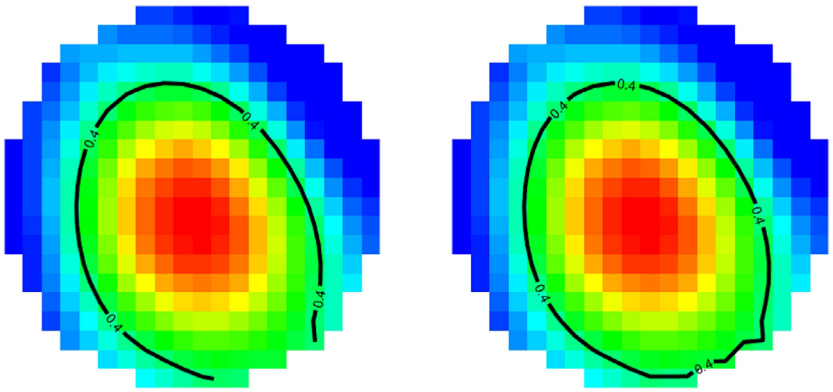

Figure 8. Identification of the boundary between a large bubble and liquid in a open contour (the left), and a closed contour with a physical boundary (the right).

segments during the interrogation. Those neighbouring cells with high gas concentration should be merged together to form a large bubble.

After a cluster of the cells is located to form a large bubble, isofurface algorithm, e.g. Marching cubes [32], is applied to extract the interface between the bubble and liquid. Suppose a cell with the values of all vertices are larger than a given threshold, but this cell is located at a physical boundary, e.g. pipe wall, the algorithm, unfortunately, will not respect that there should have an isosurface segment as the physical boundary. The left image in figure 8 shows an example of an open contour, with a black contour of 0.4. It clearly demonstrates that without the consideration of the physical boundary, the contour becomes open, which is obviously inconsistent with reality. As a result, the algorithm has to be enhanced to reflect this situation. The right image in figure 8 illustrates an example of the application of enhanced isosurface algorithm with the consideration of the physical boundary.

3. Evaluation

The proposed approach is evaluated using concentration tomograms by ERT systems, on an industrial gas–liquid flow in both vertical and horizontal pipelines, covering almost all typical flow regimes in gas–liquid flow[3]. For each flow regime, three images are presented by high-speed camera, conventional colour mapping, and the proposed approach. All colour mappings of concentration are generated using the same colour mapping (from blue to red) and the same scale (0%, 100%). The local velocity of the gas phase was calculated by the aforementioned online cross-correlation method

[3] The results exclude churn flow, not for lack of applicability of the approach, but for lack of corresponding image/video.

Table 1. Selected conditions for horizontal pipeline flow.

V_g (m s^{-1})	V_w (m s^{-1})	GVF (%)	Observed flow regime	Total frames
0.114	0.026	81.67	Stratified flow	3900
0.064	1.232	4.94	Bubbly flow	6900
0.136	0.754	15.31	Plug flow	3300
0.541	0.353	60.54	Slug flow	1300
4.483	0.066	98.54	Annular flow	100

or the superficial velocity of gas phase when the method is inapplicable. When the method is applied, the cross-correlation length is fixed at 4000 frames, and the moving window is fixed at 500 frames. In order for the comparison to be more reasonable, all images for a given pipe orientation were generated to represent the same length, i.e. the distance of the flow passed through the pipe. Therefore, the total frames needed for generating the images reflecting the same travel distance of each flow condition can be derived by:

$$AF = \sum_{i=1}^{n} \frac{\text{Dist} \times \text{DAS}}{v_i} \tag{12}$$

where Dist is the travelling distance of the flow, DAS is the data acquisition speed of the ERT, and v_i is the mean pixel velocity of the gas phase by the online cross-correlation method or the superficial velocity of the gas phase.

3.1. Gas–liquid flow in horizontal pipeline

A set of experiments was conducted in a horizontal pipeline with diameter of 200 mm on the flow testing facilities at TUV NEL, and the data was gauged by a commercialised ERT system, namely V5R [6], at the speed of 312.5 dual frames per

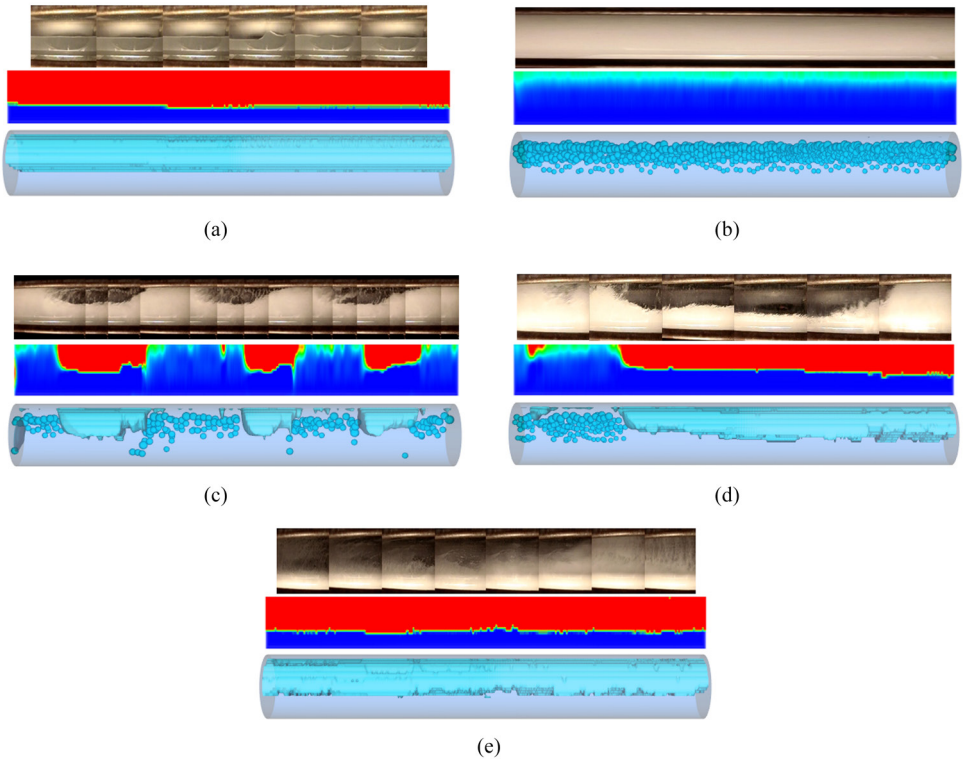

Figure 9. Visualisation of gas–liquid flow travelling 1.4 m (the flow direction from right to left) in a horizontal pipe by a high-speed camera , conventional colour mapping and proposed bubble mapping. (a) stratified flow; (b) bubble flow; (c) plug flow; (d) slug flow; and (e) annular flow.

second (dfps). The mesh resolution of the 2D tomograms by V5R is 20×20. The actual travelling distance reflected by the images is 1.4 m. The selected flow conditions for the evaluation are listed in table 1, where flow reference of water superficial velocity, gas superficial velocity, and GVF (Gas volume fraction) were provided by the testing facilities. According to (12) and the actual flowing distance (1.4 m), the total frames for generating the images are listed in table 1. Since the local velocity of stratified (wavy) and annular flow is not derivable using the cross-correlation method, the superficial velocity is therefore applied to approximate the local velocity of the gas phase for these two flow regimes. Another point is that the error by measuring pure liquid is less than 3% during the experiment. Consequently, 3%, instead of 5% is chosen for T_l.

Given the above parameters/thresholds, visualisation results based on the bubble mapping are depicted in figure 9, along with the images from a high-speed camera taken through a photo chamber and the visualisation by conventional colour mapping. For a stratified flow in figure 9(a), the flow regime can be clearly recognised by all images. The situation changes when coming to a bubbly flow as shown in figure 9(b). The images by the high-speed camera and the colour mapping are incapable of visualising the small bubbles in the bubbly flow, whereas the bubble mapping shows how the small bubbles distribute in the pipe. For a plug flow (figure 9(c)) and a slug flow (figure 9(d)), the camera and the colour mapping present similar results, i.e. the large bubbles can be located but the small bubbles are missing, whereas the bubble mapping complement the limitations by the methods. As far as annular flow is concerned, both the colour mapping and the bubble mapping are unable to demonstrate the thin water film at the top of the pipe. This is because the film is too thin to be identified by ERT system.

Table 2. Selected conditions for vertical pipeline flow.

V_g (m s^{-1})	V_w (m s^{-1})	GVF (%)	Observed flow regime	Total frames
0.085	0.878	8.83	Bubbly flow	4400
0.51	0.57	47.22	Slug flow	800
18.42	0.035	99.81	Annular flow	100

3.2. Gas–liquid flow in vertical pipeline

Another set of experiments was performed for an upward gas–liquid flow in a 50 mm vertical section of the flow loop in the University of Leeds. 20×20 cross-sectional concentration data was obtained by another commercialised ERT system, called FICA [5], at the speed of 1000 dfps, and later stacked sequentially to form a 3D concentration dataset. The selected conditions for the evaluation are listed in table 2. In the images, the flow travels 0.4 m, and hence the total frames for each condition to generate the flowing distance are also listed in the table. As the aforementioned reason, the local velocity of the annular flow is replaced using the superficial velocity of the gas phase. 40% is used for T_g and 5% for T_l. The visualisation results, including bubbly flow, slug flow, and annular flow are presented in figure 10, accompanied with concatenated images by high-speed camera and colour-based rendering.

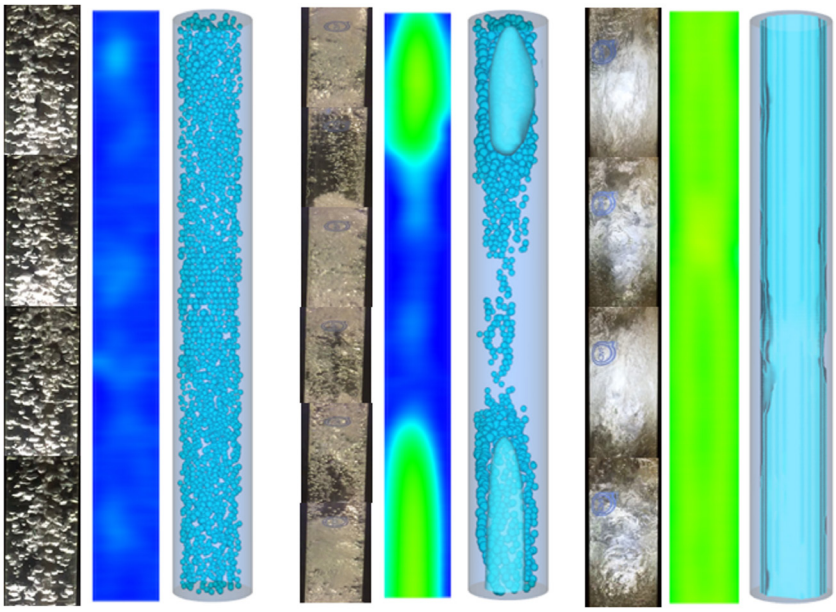

Figure 10. Visualisation of upward gas–liquid flow moving 0.4 m in a vertical pipe by a high-speed camera, conventional colour mapping and proposed bubble mapping. (a) bubbly flow; (b) slug flow; and (c) annular flow.

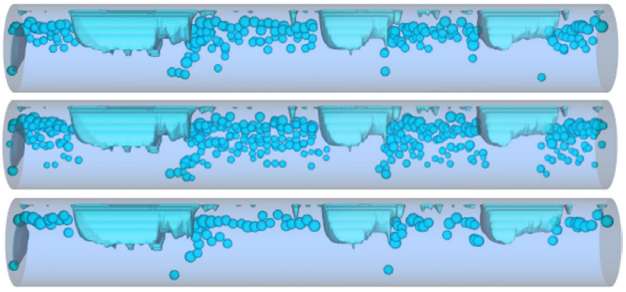

Figure 11. Visualisation results by different T_l of 5%, 2%, and 8% (from the top to the bottom).

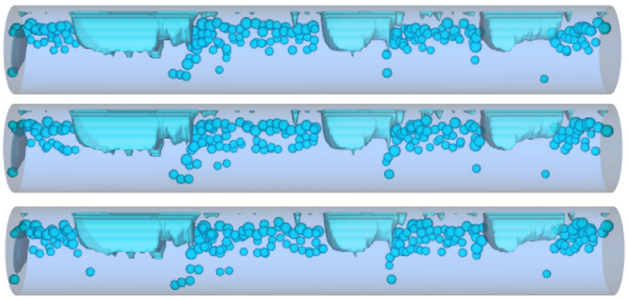

Figure 12. Visualisation results by different T_g of 40%, 50%, and 60% (from the top to the bottom).

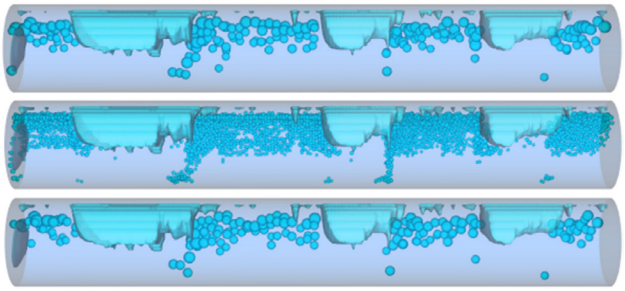

Figure 13. Visualisation results by different IC of 4 × 4, 2 × 2, and 5 × 5 (from top to bottom).

The resultant visualisation of a bubbly flow in a vertical pipe is different from the one in a horizontal pipe, as depicted in figures 9(b) and 10(a). In each group of images, e.g. figure 9(b), the top shows the photo from camera, the middle is the axial cross section of stacked tomograms, and the bottom shows the image produced by the bubble mapping approach. It is clearly demonstrated that both the camera and the bubble mapping can visualise the small bubbles, whereas the colour mapping does not. For a slug flow (figure 10(b)), the flow regime can be recognized, but it is a little challenging to locate the exact size and distribution of the large bubbles due to the existence of small bubbles using the camera, whereas the stacked tomogram illustrates the approximate size and position of the large bubbles. In contrast, the bubble mapping reveals the small and the large bubbles. When it comes to an annular flow (figure 10(c)), both the camera and the tomogram can show the flow regime, but struggle to reflect the thickness of the liquid film surrounding the gas, whereas the bubble mapping can.

3.3. Impact of the critical parameters

Since the parameters, i.e. T_g, T_l, and IC dimensions, are critical for the approach, the impact of the values on the results is evaluated. For each parameter, three different values are selected, and corresponding visualisation results are presented, while

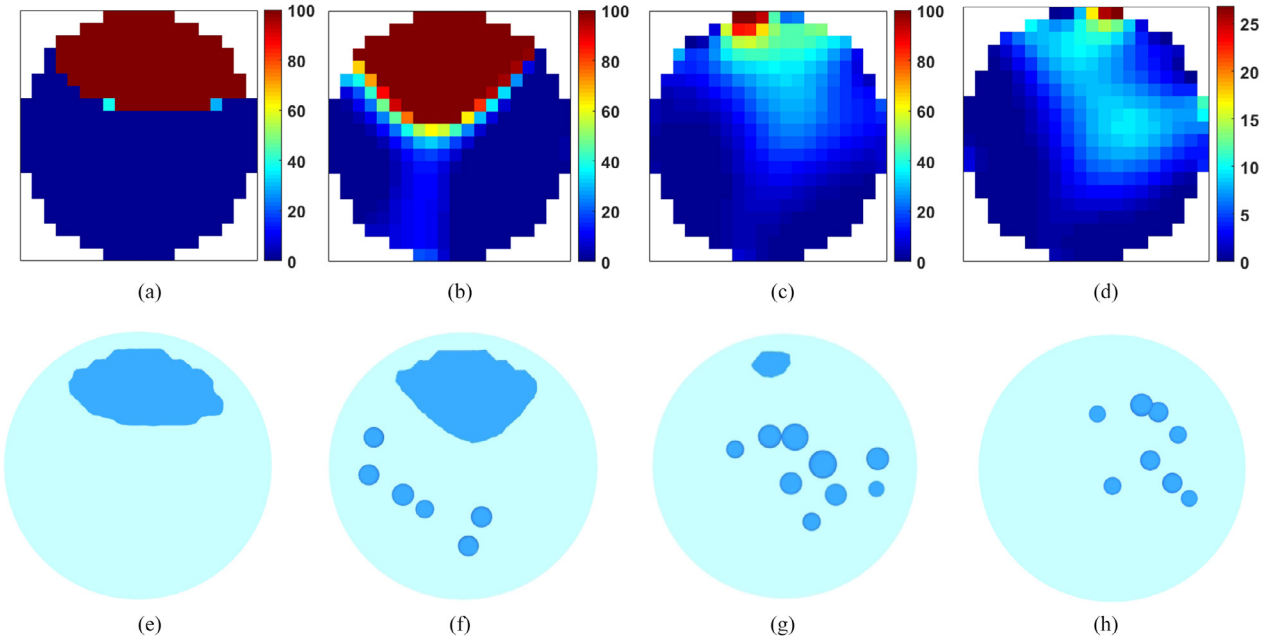

Figure 14. Cross-sectional images of ERT tomograms (the top) and bubble mapping results (the bottom) for the plug flow with a large bubble ((a) and (e)), a large bubble with small bubbles ((b) and (f)), tail of a large bubble with small bubbles ((c) and (g)), and small bubbles ((d) and (h)).

keeping the other parameters unchanged. Plug flow in horizontal pipeline (figure 9(c)) is chosen for the demonstration because it contains both small and large bubbles.

Figure 11 depicts the influence of the threshold for pure liquid T_l on the visualisation. The original rendering with $T_l = 3\%$, i.e. the top one in the figure, is set as the reference, and two more renderings with $T_l = 2\%$ (the middle one) and $T_l = 8\%$ (the bottom one) are generated. In the renderings, 174, 245, and 79 small bubbles are reconstructed, respectively, whereas the number of large bubbles is unchanged. In consequence, the threshold T_l affects the number of reconstructed small bubbles, but does not affect the large bubbles, mainly because the threshold determines the proportion of liquid phase. That is, the higher the threshold is, the less the liquid is, and in turn the more the gas is.

The effect of the threshold T_g is presented in figure 12, in which three different values, including 40%, 50%, and 60%, are applied, and the outcomes are from top to bottom respectively. From visualisation point of view, the change does not have a distinguishable effect on the outcomes. The number of acknowledged small bubbles also proves it, in which there are 174, 174, and 183 small bubbles, respectively. Since T_g determines the full occupation of an IC by gas, it is crucial to the volume of large bubbles, and the boundaries between large bubbles and liquid, although the figure does not explicitly illustrate it.

Another important parameter is the dimensional definition of IC, and figure 13 shows the comparison. In essence, the size of IC is vital for the size of small bubbles, since the volume is not beyond an IC. In addition, it also influences the number of mapped small bubbles, since smaller IC results in more amount of IC with a given concentration distribution. Consequently, the smallest IC results in the bubbles of the smallest in size and the most in number, as shown by the middle one in figure 13, in which totally 3251 small bubbles are located with the IC of 2×2 spatial dimension, compared to the ones by the IC of 4×4 and 5×5 with 174 and 158 small bubbles, respectively. In contrast, the appearance of large bubbles is irrelevant to the parameter.

Table 3. Mean air concentrations of selected cross-sectional images from ERT and bubble mapping.

	Case 1 (%)	Case 2 (%)	Case 3 (%)	Case 4 (%)
ERT	30.91	33.91	14.38	5.66
Bubble mapping	29.64	24.59	10.68	3.85

3.4. Quantitative analysis of plug flow

Four cross-sectional images at different positions at the plug flow (figure 9(c)) are chosen for quantitative comparison. They are a large bubble, a large bubble with small bubbles, tail of a large bubble with small bubbles, and small bubbles. The images are demonstrated in figure 14, and mean air concentrations derived from the images are presented in table 3. It is worth noting that the cross-sectional images from the bubble mapping result includes pipe wall, but the corresponding concentration is derived excluding the wall. When there is only one large bubble, the images by ERT and bubble mapping (figures 14(a) and (e)) are similar, and the mean gas concentrations are very close (Case 1 in table 3). This is mainly because of the application of SBP reconstruction which makes the boundary between the large bubble and liquid sharp. When small bubbles are introduced, both images and mean gas concentration are different. As far as mean gas concentration is

concerned, bubble mapping results tend to underestimate it. This is primarily because of the assumption of noise, i.e. mean concentration less than 5% is assumed due to noise and therefore ignored.

4. Conclusion

A novel approach, namely bubble mapping, has been proposed to visualise gas–liquid flow based on electrical concentration tomograms. With the reasonable assumptions, small bubbles can be reconstructed and large bubbles can be located by a bubble lookup table. Small bubbles are randomly located in a cubic volume, and their sizes are fractional to the mean concentrations of air in the cubes. In contrast, large bubbles are random in shape and location, reconstructed by a cluster of neighbouring cubes with the local mean concentrations beyond a threshold value and an enhanced isosurface approach. The evaluational results demonstrated that through this approach, colour-based flow phase distributions are transformed to bubble-based visualisation, which is capable of significantly improving flow regime visualisation and visual recognition, and thus eliminating the visual ambiguities caused by the conventional colour mapping-based approaches. In addition, the bubble mapping results are able to convey more detailed information which the colour mapping ones are not, e.g. the bubble size increases when they are closer to the upper wall of the pipe in horizontal flow (e.g. figure 9(b)). It is worth noting that when large bubbles are involved, the overall mean concentration is not conserved any more due to the threshold value selected is 0.4, rather than 1.0, which may result in the overestimation of large bubble size. However, it has little influence on the visualisation and visual recognition of flow regimes.

Despite of the feasibility of the proposed approach, there are still a few aspects to be addressed in the future studies. The threshold value used for classifying small bubbles and large bubbles in the bubble lookup table needs to be studied for the theoretical support, e.g. determining the value with an inverse method [33]. Since the visual results are dependent on the quality of input data, i.e. the spatial resolution of electrical concentration tomograms, the resultant visualisation could be improved by applying advanced algorithms in both tomography and computer graphics, such as the one by [15, 34], respectively. However, the challenge still remains in overcoming the underestimation error from imaging of large non-conductive object with the current status of ERT. It is also worthwhile to indicate the potential artefact introduced, particularly the small bubbles appeared around a distinctive large bubble, which is caused by the point-spread effect of the tomographic imaging although they are not playing a predominant role in flow regime visualisation.

Acknowledgment

This work is funded by the Engineering and Physical Sciences Research Council (EP/H023054/1), the European Metrology Research Programme (ENG58-MultiFlowMet) project ‘Multiphase flow metrology in the Oil and Gas production’, and the European Metrology Programme for Innovation and Research project (16ENG07-MultiFlowMet II) project multiphase flow reference metrology, which are jointly funded by the European Commission and participating countries within Euramet and the Europea union.

ORCID iDs

Qiang Wang https://orcid.org/0000-0002-1665-7408

References

[1] Corneliussen S, Couput J-P, Dahl E, Dykesteen E, Frøysa K-E, Malde E, Moestue H, Moksnes P O, Scheers L and Tunheim H 2005 *Handbook of Multiphase Flow Metering* (Oslo: Norwegian Society for Oil and Gas Measurement)
[2] Brennen C E 2005 *Fundamentals of Multiphase Flows* (Cambridge: Cambridge University Press)
[3] Wang M (ed) 2015 *Industrial Tomography Systems and Applications* (Cambridge: Woodhead Publishing) (https://doi.org/10.1016/C2013-0-16466-5)
[4] Prasser H-M, Scholz D and Zippe C 2001 Bubble size measurement using wire-mesh sensors *Flow Meas. Instrum.* **12** 299–312
[5] Wang M, Ma Y, Holliday N, Dai Y, Williams R A and Lucas G 2005 A high-performance EIT system *IEEE Sensors J.* **5** 289–99
[6] Jia J, Wang M, Schlaberg H I and Li H 2010 A novel tomographic sensing system for high electrically conductive multiphase flow measurement *Flow Meas. Instrum.* **21** 184–90
[7] Cui Z, Wang H, Chen Z, Xu Y and Yang W 2011 A high-performance digital system for electrical capacitance tomography *Meas. Sci. Technol.* **22** 055503
[8] Wang M, Dickin F J and Mann R 1999 Electrical resistance tomography sensing systems for industrial applications *Chem. Eng. Commun.* **175** 49–70
[9] Dickin F and Wang M 1996 Electrical resistance tomography for process applications *Meas. Sci. Technol.* **7** 247–60
[10] Maxwell J C 1982 *A Treatise on Electricity and Magnetism* vol 1, 3rd edn (Oxford: Oxford University Press)
[11] Williams R A *et al* 1999 Industrial monitoring of hydrocyclone operation using electrical resistance tomography *Miner. Eng.* **12** 1245–52
[12] Hastie T, Tibshirani R and Friedman J 2009 *The Elements of Statistical Learning* (Berlin: Springer)
[13] Aykroyd R G 2015 15—statistical image reconstruction *Industrial Tomography* (*Woodhead Publishing Series in Electronic and Optical Materials*) ed M Wang (Cambridge: Woodhead Publishing) pp 401–27
[14] Chen X, Hu H, Liu F and Gao X X 2011 Image reconstruction for an electrical capacitance tomography system based on a least-squares support vector machine and a self-adaptive particle swarm optimization algorithm *Meas. Sci. Technol.* **22** 104008
[15] Wang M 2002 Inverse solutions for electrical impedance tomography based on conjugate gradients methods *Meas. Sci. Technol.* **13** 101–17
[16] Hansen C D and Johnson C R 2011 *Visualization Handbook* (Amsterdam: Elsevier) (https://doi.org/10.1016/B978-012387582-2/50030-7)
[17] Manera A, Prasser H-M, Lucas D and van der Hagen T H J J 2006 Three-dimensional flow pattern visualization and

bubble size distributions in stationary and transient upward flashing flow *Int. J. Multiph. Flow* **32** 996–1016
[18] Ye L and Yang W 2012 Real-time 3d visualisation in electrical capacitance tomography *2012 IEEE Int. Conf. on Imaging Systems and Techniques* pp 40–4
[19] Jia J, Wang M and Faraj Y 2015 Evaluation of eit systems and algorithms for handling full void fraction range in two-phase flow measurement *Meas. Sci. Technol.* **26** 015305
[20] ITS 2009 *ITS System 2000 Version 7.0 p2+ Electrical Resistance Tomography System—User's Manual* (Manchester: Industrial Tomography Systems Plc.)
[21] Guet S, Ooms G and Oliemans R V A 2002 Influence of bubble size on the transition from low-re bubbly flow to slug flow in a vertical pipe *Exp. Therm. Fluid Sci.* **26** 635–41
[22] Sanders R S, Razzaque M M, Schaan J, Nandakumar K, Masliyah J H, Afacan A and Liu S 2004 Bubble size distributions for dispersed air-water flows in a 100 mm horizontal pipeline *Can. J. Chem. Eng.* **82** 858–64
[23] Jin H, Wang M and Williams R A 2007 Analysis of bubble behaviors in bubble columns using electrical resistance tomography *Chem. Eng. J.* **130** 179–85
[24] Qi F S, Yeoh G H, Cheung S C P, Tu J Y, Krepper E and Lucas D 2012 Classification of bubbles in vertical gas–liquid flow: part 1—an analysis of experimental data *Int. J. Multiph. Flow* **39** 121–34
[25] Tan J and Yang X 2009 Physically-based fluid animation: a survey *Sci. China* F **52** 723–40
[26] Beck M S and Plaskowski A 1987 *Cross Correlation Flowmeters, their Design and Application* (London: Taylor and Francis)
[27] Dong F, Xu Y B, Xu L J, Hua L and Qiao X T 2005 Application of dual-plane ert system and cross-correlation technique to measure gas–liquid flows in vertical upward pipe *Flow Meas. Instrum.* **16** 191–7
[28] Wang M, Jia J, Faraj Y, Wang Q, Xie C, Oddie G, Primrose K and Qiu C 2015 A new visualisation and measurement technology for water continuous multiphase flows *Flow Meas. Instrum.* **46** 204–12
[29] Ma Y, Holliday N, Dai Y, Wang M, Williams R A and Lucas G 2003 A high performance online data processing eit system *3rd World Congress on Industrial Process Tomography (Banff, Canada)*
[30] Wang M, Jia X, Bennett M and Williams R A 2001 Flow regime identification and optimum interfacial area control of bubble columns using electrical impedance imaging *2nd World Congress on Industrial Process Tomography* pp 726–34
[31] Deckwer W-D 1992 *Bubble Column Reactors* (New York: Wiley)
[32] Lorensen W E and Cline H E 1987 Marching cubes: a high resolution 3d surface construction algorithm *SIGGRAPH Comput. Graph.* **21** 163–9
[33] Li K, Wang Q, Wang M, Yang N and Han Y 2018 Imaging of a distinctive large bubble in gas-water horizontal flow based on size projection algorithm *9th World Congress on Industrial Process Tomography* (ISIPT)
[34] Anderson J C, Garth C, Duchaineau M A and Joy K I 2010 Smooth, volume-accurate material interface reconstruction *IEEE Trans. Vis. Comput. Graphics* **16** 802–14